JACS Au
AN OPEN ACCESS JOURNAL OF THE AMERICAN CHEMICAL SOCIETY

pubs.acs.org/jacsau

Article

Hydrocarbon Products Occluded within Zeolite Micropores Impose Transport Barriers that Regulate Brønsted Acid-Catalyzed Propene Oligomerization

Elizabeth E. Bickel and Rajamani Gounder*

Cite This: *JACS Au* 2022, 2, 2585−2595

Read Online

ACCESS | Metrics & More | Article Recommendations | Supporting Information

ABSTRACT: Brønsted acid zeolites catalyze alkene oligomerization to heavier hydrocarbon products of varied size and branching. Propene dimerization rates decrease monotonically with increasing crystallite size for MFI zeolites synthesized with fixed H^+-site density, revealing the strong influence of intrazeolite transport limitations on measured rates, which has gone unrecognized in previous studies. Transient changes in dimerization rates upon step-changes in reactant pressure (150−470 kPa C_3H_6) or temperature (483−523 K) reveal that intrazeolite diffusion limitations become more severe under reaction conditions that favor the formation of heavier products. Together with effectiveness factor formalisms, these data reveal that product and reactant diffusion, and consequently oligomerization rates and selectivity, are governed by the composition of hydrocarbon products that accumulate within zeolitic micropores during alkene oligomerization. This occluded organic phase strongly influences rates and selectivities of alkene oligomerization on medium-pore zeolites (MFI, MEL, TON). Recognizing the coupled influences of kinetic factors and intrazeolite transport limitations imposed by occluded reaction products provides opportunities to competently tailor rates and selectivity in alkene oligomerization and other molecular chain-growth reactions through judicious selection of zeolite topology and reaction conditions.

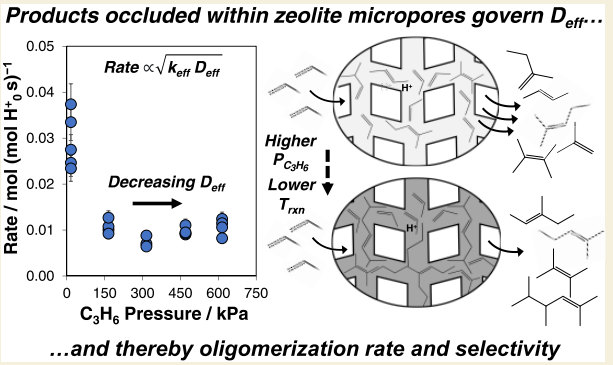

KEYWORDS: *deactivation, diffusion, zeolites, oligomerization, heterogeneous catalysis*

1. INTRODUCTION

Brønsted acidic zeolite catalysts are ubiquitous in converting carbon-based feedstocks such as methanol to olefins and hydrocarbons,[1] biomass to fuels and chemicals,[2,3] alkane cracking to lighter hydrocarbons,[4,5] and alkene oligomerization to transportation fuel-range molecules.[6−8] Zeolites are inorganic crystalline frameworks that confine acid sites (H^+) within microporous voids. The sizes and shapes of these voids influence the intrinsic kinetic behavior of H^+ sites[9,10] and also regulate the diffusion of reactant and product molecules, as well established in concepts of shape selectivity.[4,11,12] The coupled effects of H^+-site reactivity and diffusional constraints imposed by the inorganic zeolitic framework are well documented to influence rates, selectivity, and catalyst lifetime for various zeolite-catalyzed reactions including toluene disproportionation,[13] *n*-heptane isomerization,[14] *n*-paraffin cracking,[15] methanol to olefins and hydrocarbons,[16−19] and cumene synthesis.[20] This recognition has spurred advances in the synthesis and modification of zeolite crystallites with altered diffusion properties, including engineering changes in crystal size and habit, mesoporosity, and crystallite-scale H^+-site distributions.[21−28] Here, we provide evidence that additional transport barriers are imposed by an organic phase composed of hydrocarbon products that accumulate within the micropores of medium-pore (e.g., 10-membered ring, 10-MR) zeolites during alkene oligomerization reactions.

Propene oligomerization on Brønsted acid zeolites proceeds via a complex reaction network to form alkene products of varied size and branching. Selectivities to higher-molecular-weight products (e.g., C_9) and isomers with high degrees of branching (e.g., 2,3-dimethylbutene) have been proposed to depend on properties of 10-MR zeolites (e.g., pore connectivity, crystallite size, H^+-site density) because the rate of egress of such products is restricted by diffusion barriers imposed by the inorganic zeolite framework.[22,29] In contrast, net rates of propene oligomerization (i.e., C_3 consumption) have been proposed to depend solely on zeolite properties that influence intrinsic kinetic constants for dimerization and

Received: August 22, 2022
Revised: October 3, 2022
Accepted: October 6, 2022
Published: November 1, 2022

trimerization steps (e.g., pore size, acid strength, H^+-site proximity).[30−33] Yet, prior studies report different dependences of propene oligomerization rates (per H^+, 503−533 K) on H^+-site density[30,31,33] in MFI zeolites for rates measured at different pressures (22−75 kPa C_3H_6), observations that cannot be rationalized solely by kinetic considerations.

In this work, we synthesized a suite of MFI zeolites with fixed H^+-site density (∼0.3 per unit cell (u.c.)), but with varied crystallite sizes (0.13−2.65 μm), to directly assess the relative contributions of diffusion and reaction phenomena to measured propene oligomerization rates and product selectivity. The dependence of propene oligomerization rates on crystallite size, in conjunction with effectiveness factor formalisms, reveals that rates are strongly limited by intrazeolite diffusion. Moreover, transient changes in dimerization rates upon step-changes in reaction temperature or propene pressure indicate that these diffusion limitations become increasingly severe under reaction conditions that preferentially form heavier alkene products. We show that transport barriers are imposed by hydrocarbon products that accumulate within zeolitic micropores during propene oligomerization, even at nominally differential conversions (X < 1%). Occluded hydrocarbon products reversibly change in composition in response to changes in reaction conditions, resulting in complex dependences of rate and selectivity on reaction conditions and reaction time in medium-pore zeolites, which have not been previously recognized or reported. These findings reveal that propene oligomerization rates and selectivity depend not only on the structural properties of the inorganic zeolite framework but also on the composition of occluded organic phases formed during reaction, the latter of which becomes preeminent for the medium-pore (10-MR) zeolites often chosen for practical alkene oligomerization applications.[6,8] The approach in this study also provides a general methodology through which similarly strong influences of product-imposed intrazeolite transport restrictions can be recognized in other zeolite-catalyzed molecular chain-growth reactions.

2. EXPERIMENTAL SECTION

MFI zeolites were synthesized with approximately fixed Al content (Si/Al ∼ 250) by adapting previously reported methods.[34,35] A detailed experimental procedure for the synthesis of each sample is reported in the Supporting Information (Section S1.1). Powder X-ray diffraction (XRD) and micropore volumes calculated from N_2 adsorption isotherms were used to verify the topology and crystallinity of MFI samples. Temperature-programed desorption of NH_3 was used to quantify the number of Brønsted acid sites on each sample. The fraction of proximal Al was assessed by performing an aqueous ion exchange with $Co(NO_3)_2$ solution following the procedures outlined in a previous report.[36] The amount of Al and Si present in each sample was quantified using elemental analysis. Detailed procedures for all characterization methods are discussed in the SI (Section S1.2). Propene reactions were performed in a stainless-steel tubular reactor with a gas chromatograph (GC) to analyze the effluent composition. A detailed description of the reactor setup and approaches used for product analysis are provided in the Supporting Information (Section S1.3).

3. RESULTS AND DISCUSSION

3.1. Dependence of Dimerization Rates on Crystallite Size on MFI Zeolites

MFI samples were synthesized with fixed H^+ content (H^+/u.c. ∼ 0.3, Si/Al ∼ 250) and varied crystallite sizes (0.13−2.65 μm) by adapting previously reported methods.[34,35] Crystallite size distributions for each sample were measured from SEM images (Figure 1a−d) and the average length (>40 crystallites)

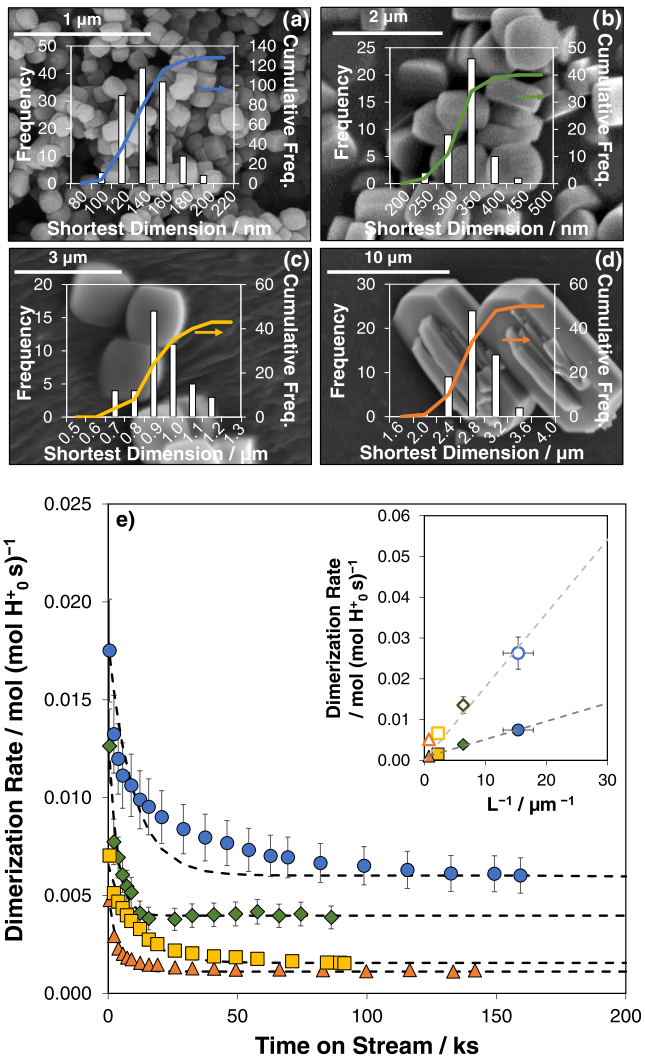

Figure 1. Representative SEM images and crystallite size distributions measured on (a) MFI-250-0.1, (b), MFI-250-0.3, (c) MFI-250-0.9, and (d) MFI-250-2.7. (e) Dimerization rates (per H_0^+) measured at 503 K and 315 kPa C_3H_6 on MFI-250-0.1 (circles), MFI-250-0.3 (diamonds), MFI-250-0.9 (squares), and MFI-250-2.7 (triangles). Dashed lines are fits to a first-order exponential decay model. Inset in (e): initial (open symbols) and steady-state (filled symbols) dimerization rates on MFI samples of Si/Al ∼ 250 plotted against inverse crystallite size (L^{-1}).

of the shortest crystallite dimension is reported as the mean crystallite size. Samples are denoted MFI-X-Y (X = approximate Si/Al, Y = mean crystallite size in μm) (Table 1). XRD patterns (Section S2, SI) and micropore volumes measured from N_2 adsorption isotherms (Section S3, SI) for MFI-X-Y samples were consistent with the MFI topology. The number of H^+ sites on each sample was quantified by NH_3 temperature-programmed desorption (TPD) (Section S4, SI)[37] to be similar to the total Al content (H^+/Al ≥ 0.91, Table S1, SI), indicating that most Al in these samples was present as framework Al. Fractions of proximal Al sites, largely comprising two Al substituted in five- and six-membered rings, were quantified using previously reported Co^{2+} titration

https://doi.org/10.1021/jacsau.2c00462
JACS Au 2022, 2, 2585−2595

Table 1. Physicochemical Properties of MFI Zeolite Samples of Dilute H^+ Content Used in This Study

sample[a]	Si/Al[b]	H^+/u.c.[c]	length[d] (μm)	std. dev.[e] (μm)
MFI-250-0.1	290	0.3	0.13	0.02
MFI-250-0.3	343	0.3	0.31	0.04
MFI-250-0.9	298	0.4	0.89	0.13
MFI-250-2.7	222	0.4	2.65	0.32

[a]Sample nomenclature is MFI-X-Y, X = approximate Si/Al ratio, Y = average length of the shortest crystallite dimension in μm. [b]Determined by ICP-OES. [c]Number of H^+-sites per unit cell (u.c.) estimated from NH_3-TPD. [d]Average length. [e]Standard deviation of the shortest crystallite dimension estimated by SEM; particle size distributions in Figure 1.

procedures[36] to be ≤ 0.08 for most samples, indicating that framework Al were predominantly isolated (Table S1, SI). Thus, these samples comprise a suite of MFI materials with essentially a fixed number of H^+ sites per unit cell (u.c.), low fractions of extra-framework Al, predominantly isolated H^+ sites, and varied crystallite size.

Scheme 1 shows a simplified reaction network for propene reactions on Brønsted acid sites that is sufficient to describe

Scheme 1. Propene Oligomerization Reaction Network on H-Zeolites[a]

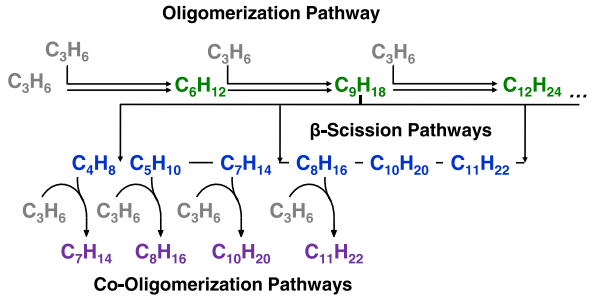

[a]Oligomerization products are defined as those whose carbon numbers are integer multiples of propene (i.e., $C_{3n}H_{2(3n)}$, n = 2, 3, 4,···) (shown in green).

product distributions observed under the conditions of this study (Section S5, SI). Propene enters the reaction network through the oligomerization pathway, which results in the formation of alkene products with carbon numbers that are integer multiples of the monomer (i.e., $C_{3n}H_{6n}$, n = 2, 3, 4,···). These oligomer products can undergo β-scission reactions to form alkenes of other carbon numbers. Propene can also enter the reaction network through co-oligomerization reactions between propene and an alkene product of a β-scission reaction,[29,38] also resulting in the formation of alkene products with carbon numbers that are not integer multiples of 3.

The rate of propene dimerization can be related to product formation rates via the stoichiometry of the reaction network (additional discussion in Section S6, SI). Dimerization rates normalized by the number of H^+ sites quantified ex situ (H_0^+) were measured at different temperatures and pressures for the MFI-250-Y samples and are shown for a representative set of reaction conditions (503 K, 315 kPa C_3H_6) in Figure 1e as a function of time-on-stream. Dimerization rates decreased with increasing time-on-stream for all H-MFI samples, regardless of the reaction conditions studied, and over the timescale of several hundred turnovers (Figure S10, SI). Such a large number of turnovers required to reach steady state is inconsistent with transient rate changes caused by equilibration of surface intermediates with external fluid-phase product concentrations, which should occur on a characteristic kinetic timescale (ca. 1 turnover), but is consistent with some form of catalyst deactivation or evolution to a less reactive state. Additionally, dimerization rates (per H_0^+) measured at fixed reaction conditions (503 K, 315 kPa C_3H_6, $X \leq 1\%$) decreased monotonically with increasing crystallite size for a given time-on-stream (Figure 1e), indicating that intracrystalline mass transfer limitations influence measured rates, since other sample properties (e.g., H^+/u.c., H^+/Al, H^+ proximity) are fixed among the suite of MFI-250-Y samples (Table S1, SI). This dependence of rate on crystallite size also could not be rationalized by differences in H^+ sites located at extracrystalline surfaces among these samples (further discussion Section S13, SI).

The relative extent of diffusion limitations on rates was further substantiated through effectiveness factor (η) formalisms. The effectiveness factor was derived in terms of the Thiele Modulus (Φ) for propene dimerization catalyzed by H-MFI samples of a slab geometry, assuming reaction rates that are intrinsically first-order in propene pressure (detailed justification and derivation in Section S9, SI). In the limit of strong diffusion limitations, the measured dimerization rate ($r_{dim,meas}$) (per H_0^+) can be expressed in terms of the fluid-phase concentration of propene (C_{3s}), the initial H^+-site density (number of H^+ sites per crystallite volume, $[H_0^+]$), the effective kinetic rate constant of dimerization (per H_0^+) (k_{eff}), the characteristic diffusion pathlength ($L/2$), and the effective intrazeolite diffusivity of propene (D_e)

$$r_{dim,meas} = \sqrt{\frac{k_{eff} D_e}{[H_0^+]}}\, C_{3s} \frac{2}{L} \quad (1)$$

Equation (1) describes the dependence of measured rates on inverse crystallite size. Initial dimerization rates were estimated by extrapolating dimerization rate transients to zero time using an exponential decay model as in previous reports[38−40] (further discussion in Section S8, SI). Steady-state dimerization rates were taken to be that measured when rates varied less than 4% over 3 ks at each reaction condition. Both steady-state and initial dimerization rates measured at fixed propene concentration increased linearly with inverse crystallite size for MFI-250-Y samples (Figure 1e, inset), consistent with eq (1) and a strong influence of intracrystalline diffusion on measured rates for all reaction times.

At first glance, intracrystalline diffusion limitations are not expected based on estimates of the Weisz-Prater criterion,[41] which appears to be satisfied (10^{-5}−$10^{-3} < 1$, Section S10, SI) for the samples in this study. Estimates of the Weisz-Prater criterion, however, depend on the value of effective molecular diffusivity, typically assumed to be the single-component effective diffusivity of the reactant in the zeolite micropores. The effective diffusivity of propene will be lower than its single-component effective diffusivity when other species physisorbed or chemisorbed within the zeolitic micropores impose barriers to diffusion,[42] as documented for coke species within MFI micropores that decrease the self-diffusivity of methane and benzene.[43−45] Decreases in the effective diffusivity of propene and products with increasing reaction time would also be consistent with the smaller slope of the linear regression for steady-state rates compared to initial rates (by ca. 4×, Figure

https://doi.org/10.1021/jacsau.2c00462
JACS Au 2022, 2, 2585−2595

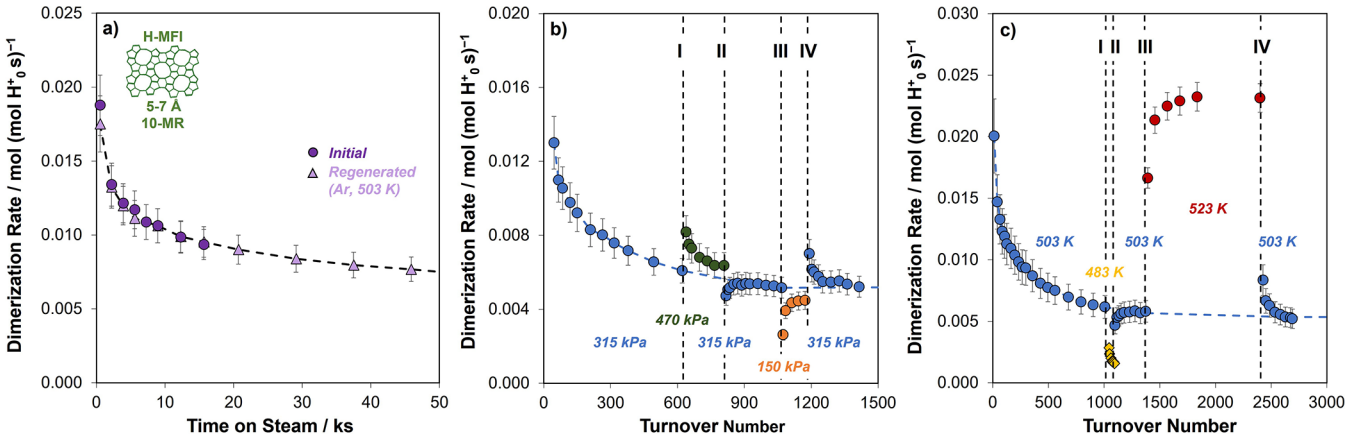

Figure 2. (a) Dimerization rates measured (503 K) initially on MFI-250-0.1 (circles) and after regeneration in flowing Ar (47 ks, triangles) at 503 K. (b) Dimerization rates measured (503 K) on MFI-250-0.1. Black dashed lines represent step-changes in the pressure. I: 315 → 470 kPa, II: 470 → 315 kPa, III: 315 → 150 kPa, IV: 150 → 315 kPa. (c) Dimerization rates measured (315 kPa C_3H_6) on MFI-250-0.1. Black dashed lines represent step-changes in the temperature. I: 503 K → 483 K, II: 483 K → 503 K, III: 503 K → 523 K, IV: 523 K → 503 K. Blue dashed lines represent an interpolation of data at 315 kPa. Error bars reflect absolute error.

1e, inset) versus inverse crystallite size (eq (1)). To assess the possibility of changes in effective intrapore diffusivity with reaction time, we next evaluate the mechanistic origin of the decrease in measured rates with time during propene oligomerization.

3.2. Mechanistic Origins of Transient Changes to Propene Oligomerization Rates upon Changes to Reaction Conditions

To identify products responsible for the decrease in measured rates with time observed during propene oligomerization, MFI samples were treated in flowing inert gas (Ar, 47 ks) at the reaction temperature (503 K) after exposure to propene (503 K, 16 ks). This inert treatment led to nearly full recovery of both initial rates (within 1.07×) and their transient decay with reaction time (Figure 2a). The removal of highly unsaturated products (e.g., polyaromatics) should have required high-temperature (>793 K) oxidative treatments;[46] moreover, the small quantity of hydride-transfer co-product alkanes (<5% for all conditions) in product distributions further indicates that aromatics were not formed in significant quantities (Section S5, SI). The ability to fully regenerate MFI samples in flowing inert gas at the reaction temperature indicates that apparent deactivation reflects the intrapore accumulation of hydrocarbon products of low degrees of unsaturation (e.g., alkenes) that are reversibly physisorbed or chemisorbed within zeolite micropores during reaction but not deactivation by irreversible H^+-site-poisoning. These conclusions are consistent with previous studies that report occluded products after alkene oligomerization on H-MFI at similar temperatures (393−548 K) predominantly consisted of large alkenes (C_{10}−C_{35}),[46,47] and the near complete removal of occluded hydrocarbons from H-MFI after propene and butene oligomerization at similar temperatures (393−548 K) upon high-temperature (673 K) inert or vacuum treatments.[46,47] Moreover, samples tested at other propene pressures could also be regenerated with an inert gas, indicating these findings are extensible over the range of reaction conditions evaluated herein (15−630 kPa C_3H_6) (Section S8, SI).

To assess the mechanism by which accumulating alkene species lead to decreases in measured rates with time on H-MFI samples during reaction, dimerization rates (503 K) were measured during step-changes in the inlet propene pressure without intervening regeneration. A step-increase in propene pressure should increase rates of oligomerization preferentially to rates of β-scission (Scheme 1) because bimolecular oligomerization reactions have higher kinetic orders in propene pressure than monomolecular β-scission reactions[29,48,49] (further discussion in Section S11, SI), in turn resulting in the formation of heavier alkene products with increasing propene pressure. Thus, step-changes in propene pressure result in varying the molecular weight of hydrocarbons formed and occluded within zeolite micropores during catalysis. A dimerization rate transient was measured at 315 kPa until the sample had reached steady state. The propene pressure was then increased to 470 kPa and held for ∼25 ks (Figure 2b, I), and then decreased to 315 kPa (Figure 2b, II) and held for ∼50 ks. Next, the propene pressure was decreased to 150 kPa (Figure 2b, III) and held for ∼25 ks, before increasing to 315 kPa (Figure 2b, IV). Dimerization rates initially increased upon increasing the pressure to 470 kPa from 315 kPa, as expected for rates that are positive-order in propene pressure,[30,31] and then continued to decrease with time-on-stream, indicating continued deactivation at this higher pressure. A subsequent decrease in the propene pressure back to the initial condition (315 kPa) led to dimerization rates that were initially lower than the steady-state rate that was measured immediately prior to the step-change increase to 470 kPa, but rates gradually increased to this value over the course of many (∼90) turnovers (Figure 2b, II). Similarly, dimerization rates decreased upon lowering the pressure to 150 kPa and increased with time (Figure 2b, III). A subsequent increase in propene pressure back to the initial condition (∼315 kPa) led to dimerization rates that were initially higher than the steady-state rate that was measured immediately prior to the step-change to 150 kPa, and rates gradually decreased to this value over the course of many (∼60) turnovers (Figure 2b, IV).

Similar experiments were also performed with step-changes in reaction temperature at fixed propene concentration (315 kPa C_3H_6). Higher temperatures favor β-scission and the formation of lighter alkene products, while lower temperatures favor the formation of higher-molecular-weight products[38,48,50] (further discussion in Section S11, SI); thus, varying

https://doi.org/10.1021/jacsau.2c00462
JACS Au 2022, 2, 2585−2595

temperature also serves to influence the molecular weight of hydrocarbons formed and occluded within the MFI micropores during oligomerization catalysis. The dimerization rate was measured at 503 K until steady state was achieved, the temperature was decreased to 483 K (Figure 2c, I) and held for ∼25 ks. The temperature was then increased back to 503 K for ∼50 ks (Figure 2c, II), increased again to 523 K (Figure 2c, III) for ∼45 ks, and decreased back to 503 K (Figure 2c, IV). Dimerization rate transients similar to those observed upon step-changes in propene pressure at fixed temperature were observed upon step-changes in reaction temperature. Dimerization rates decreased upon lowering the temperature to 483 K and continued to decrease with time, indicating continued deactivation at this lower temperature. A subsequent increase in temperature back to the initial condition (503 K) led to dimerization rates that were lower than the steady-state rate measured immediately prior to the step-change decrease to 483 K, and gradually increased over many turnovers (∼200) with time to reach the steady-state rate measured previously at 503 K (Figure 2c, II). Likewise, when the temperature was subsequently increased again from 503 to 523 K, rates gradually increased with time to reach a new pseudo-steady state (Figure 2c, III). When the temperature was decreased to 503 K, rates were initially higher than the steady-state value previously measured and decreased over many turnovers (∼120) to reach the steady-state rate previously measured at 503 K (Figure 2c, IV).

Rates that are lower than the expected steady-state rate upon a step-decrease in propene pressure or step-increase in reaction temperature and then increase with time to reach that rate indicate that the heavier hydrocarbon products formed at higher propene pressures and lower reaction temperatures inhibit dimerization rates. These heavier products gradually diffuse (or undergo β-scission and diffuse) out of crystallites over the course of many catalytic turnovers en route to establishing a lighter composition of occluded hydrocarbons that is characteristic of the lower propene pressure (Scheme 2iii–v) or higher reaction temperature. Likewise, dimerization rates that are initially higher than the expected steady-state rate upon a step-increase in propene pressure or step-decrease in reaction temperature and then gradually decrease to the expected steady-state rate indicate that the lighter intracrystalline product composition established at lower pressure (Scheme 2, vi) and higher reaction temperature gradually evolve to form the heavier intracrystalline product composition characteristic of the higher propene pressure (Scheme 2, iii) or higher reaction temperature, which inhibits dimerization rates to a greater extent.

The inhibition of dimerization rates by higher-molecular-weight products is consistent with the imposition of intrazeolite diffusional constraints on reactants and products by higher-molecular-weight products present within zeolitic micropores. Such inhibition indicates that the effective diffusivity of propene during oligomerization catalysis is much lower than the single-component effective diffusivity of propene in otherwise vacant micropores of the inorganic MFI framework and depends on the composition of the organic phase of hydrocarbon products occluded within the micropores. This explanation is also consistent with the large number of turnovers required to reach steady-state upon a step-change in propene pressure, which exceeds the kinetic timescale (ca. ∼1 turnover), and with the larger number of turnovers required to reach steady-state upon a decrease

Scheme 2. Proposed Depiction of the Changes in Alkene Products Accumulated the MFI Micropores during Propene Oligomerization upon Step-Changes in C_3H_6 Pressure at a Fixed Reaction Temperature[a]

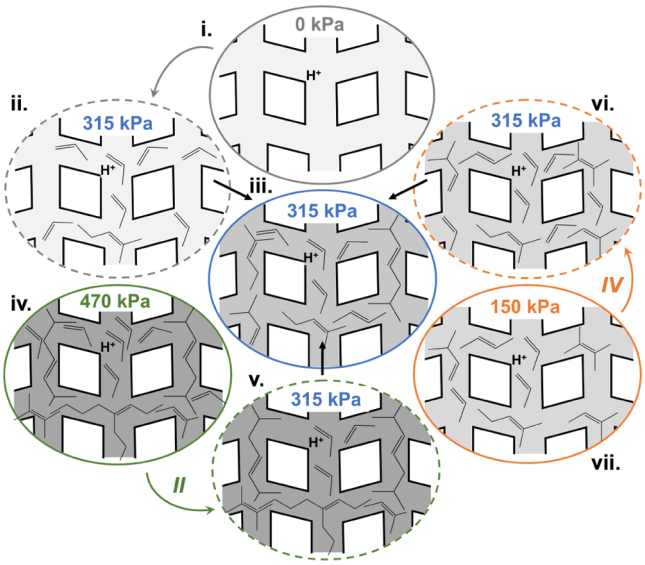

[a]Images outlined by solid lines represent the catalyst at steady state for a given pressure. Images outlined with a dashed line depict the state of the catalyst immediately following a step-change in pressure to 315 kPa from the previous state, denoted with curved arrows. (i) empty MFI pore at 0 kPa C_3H_6, the steady-state composition of occluded products expected at (iii) 315 kPa C_3H_6, (iv) 470 kPa C_3H_6, and (vii) 150 kPa C_3H_6. A depiction of the expected identity of occluded products immediately upon a step-change in C_3H_6 pressure to (ii) 0 → 315 kPa C_3H_6, (v) 470 → 315 kPa C_3H_6, and (vii) 150 → 315 kPa C_3H_6. Darker gray shading indicates that accumulated species are expected to be composed of heavier products. Italicized Roman numerals correspond to step-changes in C_3H_6 pressure in Figure 2.

compared to an increase in propene pressure or an increase compared to a decrease in reaction temperature of similar magnitude (e.g., Figure 2b, II vs IV), which indicates slower rates of diffusion at higher pressures. While inhibition of dimerization rates by heavier products could also result if such products reversibly adsorbed to active H^+ sites to increase the surface coverages of intermediates of lower reactivity, this possibility is inconsistent with transients observed in product formation rates upon pressure step-changes and with apparent reaction orders for product formation rates (further discussion Section S14, SI). Thus, we conclude that accumulated alkene products within the MFI micropores during propene oligomerization impose barriers to the intrazeolitic diffusion of propene and other products, resulting in the apparent deactivation of MFI samples with time. The composition of this occluded organic phase is sensitive to reaction conditions, leading to increased diffusional constraints at higher propene pressures and lower reaction temperatures because these conditions favor the formation of heavier products.

3.3. Influences of Occluded Hydrocarbon Products on Measured Propene Dimerization Rates at Varying Pressures

To explore the consequences of occluded hydrocarbon products for the dependence of dimerization rate on propene pressure, steady-state dimerization rates were measured over a range of propene pressures (15–630 kPa C_3H_6) at a fixed

https://doi.org/10.1021/jacsau.2c00462
JACS Au 2022, 2, 2585–2595

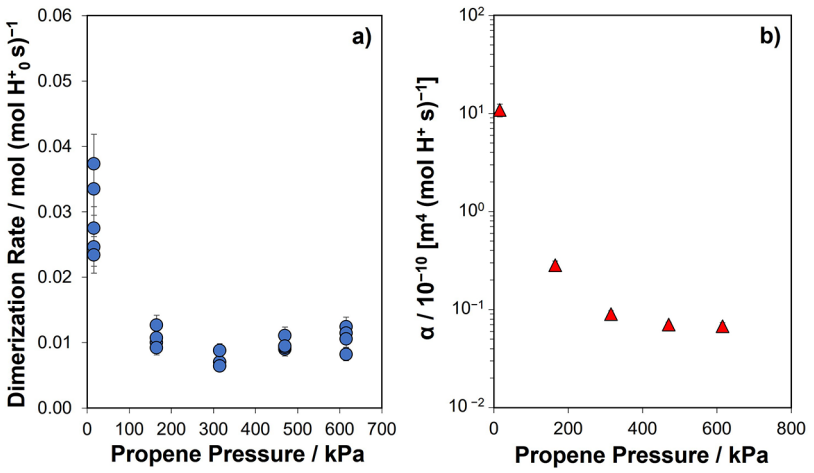

Figure 3. (a) Steady-state dimerization rates measured on MFI-250-0.1 at 503 K and varied propene pressure. Fresh catalyst was used for each measurement. (b) Values of α (eq 2) (at 503 K) from linear regressions of steady-state dimerization rates measured on MFI-250-Y samples. Error bars reflect absolute error.

temperature (503 K) on a representative MFI sample (MFI-250-0.1). Rates are plotted against propene pressure in Figure 3a. Dimerization rates decreased with increasing propene pressure in the low-pressure regime (15−315 kPa C_3H_6) but became more positive-order at higher pressures (≥470 kPa C_3H_6). A negative-order dependence of dimerization rates on propene pressure is inconsistent with kinetic rate laws derived from propene dimerization mechanisms, which predict rates will be first order in the limit of a propene- or product-covered surface (further discussion in Section S9, SI). Instead, such a negative-order dependence reflects the influence of alkene products occluded within the zeolitic micropores on reactant and product diffusion.

Higher propene pressures result in higher intrinsic rates of dimerization because kinetic rate laws are positive order in propene pressure (further discussion in Section S9, SI), but also favor the formation of increasingly heavy alkene products occluded within the catalyst micropores that result in lower effective diffusivities. To further substantiate this, dimerization rates were measured on the MFI-250-Y samples listed in Table 1 over a range of propene pressures (15−630 kPa C_3H_6), plotted against inverse crystallite size, and fit to eq 1 for each propene pressure (Figure S13, SI). A parameter α can be extracted from fits to eq 1 at each propene pressure. This parameter depends on the initial H^+-site density, which is a measurable quantity, the effective dimerization rate constant, and the effective diffusivity of propene

$$\alpha = \sqrt{\frac{k_{\text{eff}} D_e}{[H_0^+]}} \tag{2}$$

The value of α is plotted against propene pressure in Figure 3b; α decreased monotonically with increasing propene pressure over several orders of magnitude (by >10^2×, Figure 3b), indicating that the effective dimerization rate constant or effective diffusivity decreased systematically with increasing propene pressure. The effective dimerization rate constant is a function of the intrinsic kinetic rate constant for dimerization, and equilibrium constants for adsorption (eqs S38−S40, SI). This constant depends on the strength of H^+-sites (i.e., deprotonation energy) and void size,[31] but is expected to remain constant with propene pressure and among MFI samples of fixed H^+-site density (further discussion in Section S13, SI); consequently, changes in this variable cannot rationalize changes in α with propene pressure. Thus, the decreasing value of α with increasing propene pressure is best explained by a decrease in the effective diffusivity of propene. Importantly, the results of this analysis independently corroborate the results of the propene pressure step-change experiment shown in Figure 2, which also indicate products formed at higher propene pressures increasingly restrict intracrystalline diffusion. This analysis also illustrates the ability of rate measurements to assess the state of the catalyst *in operando*, which cannot be accurately inferred *ex situ* (e.g., thermogravimetric analysis on spent catalyst samples) because sample exposure to such conditions alters the quantity and composition of the occluded organics, and is further hindered by a dearth of *in situ* approaches able to distinguish among alkene products of different size and branching in the complex mixtures of products formed herein. We conclude that the convoluted pressure dependences of kinetic rates and transport limitations imposed by the intraporous organic phase results in the strong deviation of apparent rates from the expected kinetic first-order dependence on propene pressure. More positive-order dimerization rates at higher propene pressures reflect the attenuated decrease in effective diffusivity at higher propene pressures (Figure 3b). Together, these results reveal that in addition to the intrinsic kinetic rate constant dictated by properties of the inorganic zeolite framework, propene oligomerization rates are strongly influenced by the entrained organic phase composed of reaction products, which together with the inorganic framework governs the effective diffusion of propene and products.

3.4. Influence of Zeolite Topology on the Formation of an Intrazeolite Organic Phase and in turn Rates and Product Selectivity

We next evaluate the presence and influence of occluded organic phases within H-zeolites of other topologies and pore sizes (TON, MEL, *BEA, FAU), some of which are also of interest for practical alkene oligomerization processes.[51] A suite of 10-MR (TON, MEL) and 12-MR (*BEA, FAU) zeolites were obtained from commercial sources (characterization data summarized in Table S4, SI), and dimerization rates were measured at fixed conditions (503 K, 315 kPa C_3H_6) (Figure S18, SI). For each sample, dimerization rates

https://doi.org/10.1021/jacsau.2c00462
JACS Au 2022, 2, 2585−2595

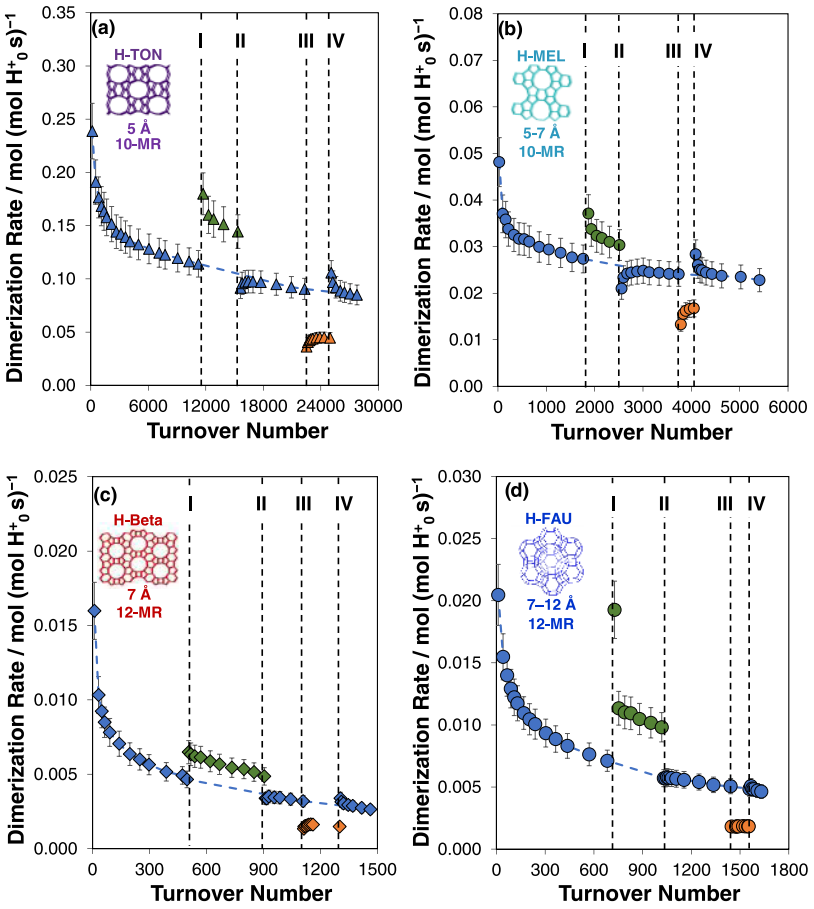

Figure 4. Pressure step-change experiments (503 K) on (a) TON, (b) MEL, (c) *BEA, and (d) FAU. Black dashed lines represent step-changes in the pressure. I: 315 → 470 kPa, II: 470 → 315 kPa, III: 315 → 150 kPa, IV: 150 → 350 kPa. Gray dashed lines represent an interpolation of pseudo-steady-state data at 315 kPa. Error bars reflect absolute error.

decreased with time-on-stream, but all samples could be regenerated (within 1.2×) with flowing inert gas (Ar, 47 ks) at reaction temperature (503 K), indicating that these zeolite topologies also deactivate due to the accumulation of alkene products (Figure S18, SI). Propene pressure step-change experiments analogous to those performed for MFI (Figure 2) were also performed for these samples (Figure 4) to evaluate the mechanism by which these alkene products led to catalyst deactivation. For MEL and TON, a step-decrease in propene pressure led to dimerization rates that were initially lower than the expected steady-state rate and increased gradually with time to reach expected values, and vice versa with a step-increase in propene pressure. Moreover, transient changes in rates upon step-changes in propene pressure persisted over many turnovers for these 10-MR topologies (Table S3). These observations, together with the regeneration experiments in inert environments, indicate the formation of an occluded organic phase within medium-pore 10-MR topologies that regulates reactant and product diffusion during oligomerization catalysis and changes in composition with propene pressure.

In sharp contrast to observations on medium-pore zeolites, transient changes in dimerization rate were not observed upon step-changes in propene pressure for large-pore 12-MR zeolites (FAU, *BEA, Figure 4c,d). The absence of transients on large-pore zeolites suggests that either products do not accumulate within the micropores of these topologies in quantities sufficient to influence intracrystalline diffusion, or that the composition of occluded products changes on a timescale faster than the first rate measurement upon a step-change in propene pressure. Either rationalization is consistent with intrazeolite diffusion limitations that are less severe for large-pore zeolites (FAU, *BEA) compared to medium-pore zeolites (TON, MFI, MEL). Notably, alleviated intrazeolite diffusion limitations for larger-pore zeolites would be expected given the lower intrinsic kinetic rate constants for FAU compared to MFI as estimated by DFT (by ca. 2× at 503 K)[31] and the higher self-diffusivities of propene in FAU than MFI (e.g., by ca. 5× at 673 K),[52] which together suggest a higher rate of diffusion relative to reaction in FAU than in MFI. Together, the transient response of dimerization rates to propene pressure step-changes among zeolites of different topologies indicates that oligomerization rates in medium-pore zeolites are governed by the composition of alkene products that accumulate within micropores during catalysis because these products restrict the diffusion of propene and products, whereas such effects are mitigated in large-pore zeolites because they facilitate the slower growth and more facile egress of heavy alkene products.

The consequences of occluded hydrocarbon products for product selectivity were assessed by measuring selectivities during catalyst deactivation at a representative set of reaction conditions (503 K, 315 kPa C_3H_6) in experiments performed at different space velocities (per H_0^+) and is plotted as a function of propene conversion for FAU and MFI (Figure 5) and for TON, MEL and *BEA (Figure S19, SI). For all topologies, the selectivity to the primary product (C_6)

https://doi.org/10.1021/jacsau.2c00462
JACS Au 2022, 2, 2585−2595

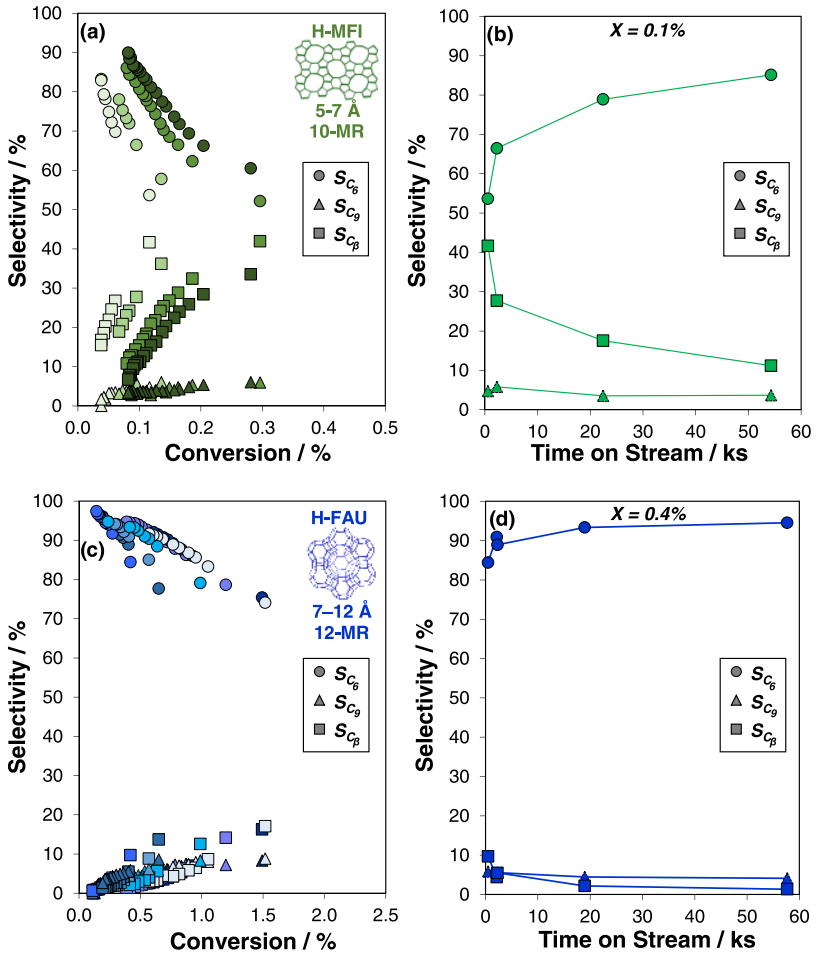

Figure 5. Selectivity to C_6 (circles) C_9 (triangles), and β-scission products (squares) measured at 315 kPa C_3H_6 and 503 K plotted against conversion for (a) MFI-250-0.1 and (c) FAU. Decreasing conversion corresponds to catalyst deactivation. Different shades of color correspond to experiments conducted at different space velocities (1−54 mol C_3 (mol H_0^+ s)$^{-1}$). Selectivity to C_6, C_9, and β-scission products at fixed conversion for samples tested at different space velocities plotted against the time-on-stream at which they were measured for (b) MFI-250-0.1 (X = 0.1%) and (d) FAU (X = 0.4%).

increased and the selectivity to higher-rank reaction products (C_9 and β-scission products) decreased with decreasing conversion. Decreasing selectivity to higher-rank products with decreasing conversion is expected when rates are kinetically controlled because higher conversions lead to higher partial pressures of the primary product at downstream positions in the catalyst bed, and thereby higher rates of formation of higher-rank products.[53] Selectivity was measured at fixed conversion and different extents of catalyst deactivation by varying the space velocity. Selectivities measured on *BEA and FAU were similar when compared at fixed conversion, regardless of time-on-stream at which the selectivity was measured (Figures 5d, S19 SI), suggesting product selectivity is influenced primarily by reactant conversion rather than the extent of catalyst deactivation. The near-invariant selectivity with extent of deactivation observed for *BEA and FAU is consistent with product formation rates that are less controlled by intrazeolite diffusion and with deactivation that occurs by a site-poisoning mechanism, because in such cases, product formation rates should depend predominantly on effective kinetic constants for their formation and on fluid-phase concentrations of propene and products, which are governed by reactant conversion.

In sharp contrast to *BEA and FAU, the selectivity to C_6 measured on MFI (Figure 5a) and MEL (Figure S19b, SI) compared at fixed conversion increased with catalyst deactivation (e.g., by ∼35% for C_6 at X ∼ 0.1% for MFI, Figure 5b), indicating that product selectivity on these topologies is strongly influenced by catalyst deactivation. Moreover, the selectivity for MFI at a given time-on-stream is similar, regardless of the corresponding propene conversion (Figure S20, SI), indicating that the increasing selectivity to C_6 with decreasing conversion is predominantly a consequence of deactivation rather than a decrease in fluid-phase propene concentration. The weaker dependence of product selectivity on conversion for MEL and MFI is consistent with strong intrazeolite diffusion limitations for these topologies. In the limit of kinetic control, higher-rank products (e.g., C_9) may form both during the egress of primary products out of the crystallite in which they were formed and from subsequent reactions within crystallites located downstream in the catalyst bed; however, the latter route will be suppressed when transport limitations disproportionately restrict larger products from diffusing into crystallites located at downstream positions in the catalyst bed. Thus, in the limit of strong intrazeolite diffusion limitations, product formation rates predominantly reflect outcomes from the sojourn of reactants and products

https://doi.org/10.1021/jacsau.2c00462
JACS Au 2022, 2, 2585−2595

through a single crystallite, thereby rendering selectivity less sensitive to fluid-phase propene conversion.

The increasing selectivity to C_6 products and decreasing selectivity to C_9 and β-scission products during the deactivation of medium-pore topologies (MFI, MEL, TON) indicates that the accumulation of hydrocarbon products within their micropores during propene oligomerization leads to the selective formation of C_6 alkenes. More severe intrazeolite diffusional constraints lead to longer intracrystalline residence times for reactants and products, and consequently should have led to higher selectivities of higher-rank products and lower selectivities to the primary product (C_6). Thus, the selective formation of C_6 during catalyst deactivation cannot solely reflect increasingly severe mass transfer limitations with catalyst deactivation, and instead suggests that occluded hydrocarbon products also influence the rates of formation of C_9 and higher-rank products relative to the rates of formation of dimers, possibly by restricting the amount of void space available for the formation of larger transition states (e.g., C_9, C_{12}). The influence of the occluded organic phase on the formation of larger transition states (e.g., C_9) suggests that this phase might also influence the stability of the dimerization transition state, and consequently the effective kinetic rate constant for dimerization (further discussion in Section S16, SI). Overall, the dependence of selectivity on time-on-stream observed for medium-pore zeolites reveals the critical role of the organic phase occluded within zeolitic micropores during propene oligomerization in governing the rates of product formation and thereby product selectivity for these topologies.

4. CONCLUSIONS

Herein, the synthesis of zeolite samples with varied crystallite size (0.13−2.65 μm) and fixed active site density in the limit of H^+-site isolation (~0.3 per u.c.), together with kinetic studies conducted over a wide range of reaction conditions (483−523 K, 15−630 kPa C_3H_6), revealed the critical and ubiquitous influence of intrazeolite diffusional constraints on the rates and product selectivity of propene oligomerization on MFI zeolites. Effectiveness factor formalisms and Weisz-Prater criterion analyses indicate that such diffusional constraints arise because of the formation of an intrazeolite organic phase, which decreases the effective diffusivity of propene and alkene products within zeolite micropores during reaction. Complete regeneration of catalysts after treatment in inert gas at reaction temperature, together with transient changes in rate in response to propene pressure and temperature step-changes, indicate that the composition of this organic phase changes reversibly in response to changes in reaction conditions, becoming heavier in composition with increasing propene pressure and decreasing reaction temperature. Consequently, effective diffusivities of propene and products monotonically decrease (>10^2×) with increasing propene pressure (15−630 kPa), leading to a complex dependence of rates on propene pressure that cannot be rationalized by mechanism-derived kinetic rate laws alone. The occluded organic phase also restricts the growth and egress of heavier oligomers (e.g., C_9), resulting in selectivities to C_6 that monotonically increase with increasing extent of deactivation.

Analogous regeneration and propene pressure step-change experiments performed on zeolites of other topologies (TON, MEL, *BEA, FAU) reveal that occluded hydrocarbons impose strong intrazeolite diffusional constraints and thereby influence rates and product selectivity for other medium-pore (10-MR) zeolites (MEL, TON). In contrast, such effects are attenuated on large-pore (12-MR) zeolites (*BEA, FAU), likely because larger micropores facilitate the slower growth and faster egression of bulky and higher-molecular-weight products. Consequently, the product selectivity on a given large-pore zeolite sample is governed predominantly by reactant conversion, which governs fluid-phase product concentrations.

Overall, these findings demonstrate that oligomerization rates and selectivities on medium-pore zeolites depend not only on the properties of the zeolite framework that govern kinetic rate constants and on the transport barriers characteristic of a given zeolite topology but also on the identity of a pernicious organic phase composed of alkene products that forms within catalyst micropores during reaction and imposes diffusional constraints on propene reactants and alkene products. In contrast to deactivation through a site-poisoning or pore-blocking mechanism, the observed decreases in reaction rate with time-on-stream during alkene oligomerization reflect the evolution of this occluded organic phase to a steady-state composition. The composition of occluded products depends on reaction conditions, leading to transient changes in rates that persist over many turnovers upon step-changes in reaction conditions that alter relative rates of chain growth and β-scission (e.g., propene pressure, temperature), reflecting the gradual evolution of the occluded organic phase to a steady-state composition characteristic of the new reaction conditions. Consequently, rates and selectivities of propene oligomerization cannot be interpreted as kinetic in origin when this occluded organic phase is present, even at low reactant conversions and the earliest stages of reaction.

These new insights into the working state of zeolite catalysts during alkene oligomerization reaction conditions reveal that the consequences of both catalyst properties and the composition of the intrazeolite organic phase formed *in-situ*, which depends on the specific reaction conditions chosen, should be considered in strategies to design and operation of more efficacious alkene oligomerization catalysts. More broadly, these findings show that intrapore diffusional constraints in zeolite-catalyzed reactions can arise not only from the inorganic zeolite framework but also from occluded products, even in topologies where such constraints are not expected from single-component effective diffusivities of the reactant because heavier product molecules that diffuse slowly out of zeolite micropores persist in the zeolitic micropores during steady-state catalysis and restrict the effective diffusivities of other species. Such phenomena are also expected to influence rates and selectivities of other classes of molecular chain-growth reactions (e.g., aldol condensation, Fisher−Tropsch synthesis) that take place within confined porous environments and reactions for which intrazeolite diffusion is known to influence measured rates (e.g., methanol to olefins).[18,19]

■ ASSOCIATED CONTENT

Supporting Information

The Supporting Information is available free of charge at https://pubs.acs.org/doi/10.1021/jacsau.2c00462.

Hydrothermal synthesis methods to prepare MFI zeolites (Section S1); full description of characterization methods (XRD, N_2 adsorption, NH_3 temperature-programmed desorption, elemental analysis), as well as

https://doi.org/10.1021/jacsau.2c00462
JACS Au 2022, 2, 2585−2595

protocol for measuring propene oligomerization rates, supplemental figures, and discussion (PDF)

AUTHOR INFORMATION

Corresponding Author

Rajamani Gounder − *Charles D. Davidson School of Chemical Engineering, Purdue University, West Lafayette, Indiana 47907, United States;* orcid.org/0000-0003-1347-534X; Email: rgounder@purdue.edu

Author

Elizabeth E. Bickel − *Charles D. Davidson School of Chemical Engineering, Purdue University, West Lafayette, Indiana 47907, United States*

Complete contact information is available at: https://pubs.acs.org/10.1021/jacsau.2c00462

Author Contributions

The manuscript was written through contributions of all authors, and all authors have given approval to the final version of the manuscript.

Notes

The authors declare no competing financial interest.

ACKNOWLEDGMENTS

The authors acknowledge financial support provided by the National Science Foundation under Cooperative Agreement No. EEC-1647722, which is an Engineering Research Center for the Innovative and Strategic Transformation of Alkane Resources. They thank Evan Sowinski for experimental assistance in benchmarking rates on a second reactor. They also thank Dr. Songhyun Lee and Dr. Mykela DeLuca (Purdue) for helpful technical discussions and a critical review of this manuscript. They also acknowledge helpful technical discussions with Professor David Hibbitts (University of Florida).

REFERENCES

(1) Yarulina, I.; Chowdhury, A. D.; Meirer, F.; Weckhuysen, B. M.; Gascon, J. Recent Trends and Fundamental Insights in the Methanol-to-Hydrocarbons Process. *Nat. Catal.* **2018**, *1*, 398−411.

(2) Jae, J.; Tompsett, G. A.; Foster, A. J.; Hammond, K. D.; Auerbach, S. M.; Lobo, R. F.; Huber, G. W. Investigation into the Shape Selectivity of Zeolite Catalysts for Biomass Conversion. *J. Catal.* **2011**, *279*, 257−268.

(3) Ennaert, T.; Aelst, J. V.; Dijkmans, J.; Clercq, R. D.; Schutyser, W.; Dusselier, M.; Verboekend, D.; F Sels, B. Potential and Challenges of Zeolite Chemistry in the Catalytic Conversion of Biomass. *Chem. Soc. Rev.* **2016**, *45*, 584−611.

(4) Degnan, T. F. The Implications of the Fundamentals of Shape Selectivity for the Development of Catalysts for the Petroleum and Petrochemical Industries. *J. Catal.* **2003**, *216*, 32−46.

(5) Primo, A.; Garcia, H. Zeolites as Catalysts in Oil Refining. *Chem. Soc. Rev.* **2014**, *43*, 7548−7561.

(6) Degnan, T. F., Jr. Applications of Zeolites in Petroleum Refining. *Top. Catal.* **2000**, *13*, 349−356.

(7) O'Connor, C. T.; Kojima, M. Alkene Oligomerization. *Catal. Today* **1990**, *6*, 329−349.

(8) Nicholas, C. P. Applications of Light Olefin Oligomerization to the Production of Fuels and Chemicals. *Appl. Catal., A* **2017**, *543*, 82−97.

(9) Gounder, R.; Iglesia, E. The Roles of Entropy and Enthalpy in Stabilizing Ion-Pairs at Transition States in Zeolite Acid Catalysis. *Acc. Chem. Res.* **2012**, *45*, 229−238.

(10) Gounder, R.; Iglesia, E. Effects of Partial Confinement on the Specificity of Monomolecular Alkane Reactions for Acid Sites in Side Pockets of Mordenite. *Angew. Chem., Int. Ed.* **2010**, *49*, 808−811.

(11) Weisz, P. B. Molecular shape selective catalysis. *Pure Appl. Chem.* **1980**, *52*, 2091−2103.

(12) Csicsery, S. M. Shape-Selective Catalysis in Zeolites. *Zeolites* **1984**, *4*, 202−213.

(13) Olson, D. H.; Haag, W. O.Structure-Selectivity Relationship in Xylene Isomerization and Selective Toluene Disproportionation. In *Catalytic Materials: Relationship Between Structure and Reactivity*; ACS Symposium SeriesAmerican Chemical Society, 1984; Vol. *248*, pp 275−307.

(14) Noh, G.; Shi, Z.; Zones, S. I.; Iglesia, E. Isomerization and *β*-Scission Reactions of Alkanes on Bifunctional Metal-Acid Catalysts: Consequences of Confinement and Diffusional Constraints on Reactivity and Selectivity. *J. Catal.* **2018**, *368*, 389−410.

(15) Haag, W. O.; Lago, R. M.; Weisz, P. B. Transport and Reactivity of Hydrocarbon Molecules in a Shape-Selective Zeolite. *Faraday Discuss. Chem. Soc.* **1981**, *72*, 317−330.

(16) Chang, C. D. Hydrocarbons from Methanol. *Catal. Rev.* **1983**, *25*, 1−118.

(17) Olsbye, U.; Svelle, S.; Bjørgen, M.; Beato, P.; Janssens, T. V. W.; Joensen, F.; Bordiga, S.; Lillerud, K. P. Conversion of Methanol to Hydrocarbons: How Zeolite Cavity and Pore Size Controls Product Selectivity. *Angew. Chem., Int. Ed.* **2012**, *51*, 5810−5831.

(18) Hwang, A.; Le, T. T.; Shi, Z.; Dai, H.; Rimer, J. D.; Bhan, A. Effects of Diffusional Constraints on Lifetime and Selectivity in Methanol-to-Olefins Catalysis on HSAPO-34. *J. Catal.* **2019**, *369*, 122−132.

(19) Shen, Y.; Le, T. T.; Fu, D.; Schmidt, J. E.; Filez, M.; Weckhuysen, B. M.; Rimer, J. D. Deconvoluting the Competing Effects of Zeolite Framework Topology and Diffusion Path Length on Methanol to Hydrocarbons Reaction. *ACS Catal.* **2018**, *8*, 11042−11053.

(20) Bellussi, G.; Pazzuconi, G.; Perego, C.; Girotti, G.; Terzoni, G. Liquid-Phase Alkylation of Benzene with Light Olefins Catalyzed by *β*-Zeolites. *J. Catal.* **1995**, *157*, 227−234.

(21) Le, T. T.; Chawla, A.; Rimer, J. D. Impact of Acid Site Speciation and Spatial Gradients on Zeolite Catalysis. *J. Catal.* **2020**, *391*, 56−68.

(22) Corma, A.; Martínez, C.; Doskocil, E. Designing MFI-Based Catalysts with Improved Catalyst Life for $C_3^=$ and $C_5^=$ Oligomerization to High-Quality Liquid Fuels. *J. Catal.* **2013**, *300*, 183−196.

(23) Le, T. T.; Shilpa, K.; Lee, C.; Han, S.; Weiland, C.; Bare, S. R.; Dauenhauer, P. J.; Rimer, J. D. Core-Shell and Egg-Shell Zeolite Catalysts for Enhanced Hydrocarbon Processing. *J. Catal.* **2022**, *405*, 664−675.

(24) Lu, P.; Ghosh, S.; Dorneles de Mello, M.; Kamaluddin, H. S.; Li, X.; Kumar, G.; Duan, X.; Abeykoon, M.; Boscoboinik, J. A.; Qi, L.; Dai, H.; Luo, T.; Al-Thabaiti, S.; Narasimharao, K.; Khan, Z.; Rimer, J. D.; Bell, A. T.; Dauenhauer, P.; Mkhoyan, K. A.; Tsapatsis, M. Few-Unit-Cell MFI Zeolite Synthesized Using a Simple Di-Quaternary Ammonium Structure-Directing Agent. *Angew. Chem., Int. Ed.* **2021**, *60*, 19214−19221.

(25) Dai, H.; Shen, Y.; Yang, T.; Lee, C.; Fu, D.; Agarwal, A.; Le, T. T.; Tsapatsis, M.; Palmer, J. C.; Weckhuysen, B. M.; Dauenhauer, P. J.; Zou, X.; Rimer, J. D. Finned Zeolite Catalysts. *Nat. Mater.* **2020**, *19*, 1074−1080.

(26) Banihashemi, F.; Ibrahim, A. F. M.; Babaluo, A. A.; Lin, J. Y. S. Template-Free Synthesis of Highly b-Oriented MFI-Type Zeolite Thin Films by Seeded Secondary Growth. *Angew. Chem., Int. Ed.* **2019**, *58*, 2519−2523.

(27) Fu, D.; Schmidt, J. E.; Ristanović, Z.; Chowdhury, A. D.; Meirer, F.; Weckhuysen, B. M. Highly Oriented Growth of Catalytically Active Zeolite ZSM-5 Films with a Broad Range of Si/Al Ratios. *Angew. Chem., Int. Ed.* **2017**, *56*, 11217−11221.

(28) Sun, M.-H.; Chen, L.-H.; Yu, S.; Li, Y.; Zhou, X.-G.; Hu, Z.-Y.; Sun, Y.-H.; Xu, Y.; Su, B.-L. Micron-Sized Zeolite Beta Single Crystals Featuring Intracrystal Interconnected Ordered Macro-Meso-Micro-porosity Displaying Superior Catalytic Performance. *Angew. Chem., Int. Ed.* **2020**, *59*, 19582−19591.
(29) Sarazen, M. L.; Doskocil, E.; Iglesia, E. Effects of Void Environment and Acid Strength on Alkene Oligomerization Selectivity. *ACS Catal.* **2016**, *6*, 7059−7070.
(30) Bernauer, M.; Tabor, E.; Pashkova, V.; Kaucký, D.; Sobalík, Z.; Wichterlová, B.; Dedecek, J. Proton Proximity − New Key Parameter Controlling Adsorption, Desorption and Activity in Propene Oligomerization over H-ZSM-5 Zeolites. *J. Catal.* **2016**, *344*, 157−172.
(31) Sarazen, M. L.; Doskocil, E.; Iglesia, E. Catalysis on Solid Acids: Mechanism and Catalyst Descriptors in Oligomerization Reactions of Light Alkenes. *J. Catal.* **2016**, *344*, 553−569.
(32) Tabor, E.; Bernauer, M.; Wichterlová, B.; Dedecek, J. Enhancement of Propene Oligomerization and Aromatization by Proximate Protons in Zeolites; FTIR Study of the Reaction Pathway in ZSM-5. *Catal. Sci. Technol.* **2019**, *9*, 4262−4275.
(33) Mlinar, A. N.; Zimmerman, P. M.; Celik, F. E.; Head-Gordon, M.; Bell, A. T. Effects of Brønsted-Acid Site Proximity on the Oligomerization of Propene in H-MFI. *J. Catal.* **2012**, *288*, 65−73.
(34) Konnov, S. V.; Dubray, F.; Clatworthy, E. B.; Kouvatas, C.; Gilson, J.-P.; Dath, J.-P.; Minoux, D.; Aquino, C.; Valtchev, V.; Moldovan, S.; Koneti, S.; Nesterenko, N.; Mintova, S. Novel Strategy for the Synthesis of Ultra-Stable Single-Site Mo-ZSM-5 Zeolite Nanocrystals. *Angew. Chem., Int. Ed.* **2020**, *59*, 19553−19560.
(35) del Campo, P.; Navarro, M. T.; Shaikh, S. K.; Khokhar, M. D.; Aljumah, F.; Martínez, C.; Corma, A. Propene Production by Butene Cracking. Descriptors for Zeolite Catalysts. *ACS Catal.* **2020**, *10*, 11878−11891.
(36) Nimlos, C. T.; Hoffman, A. J.; Hur, Y. G.; Lee, B. J.; Di Iorio, J. R.; Hibbitts, D. D.; Gounder, R. Experimental and Theoretical Assessments of Aluminum Proximity in MFI Zeolites and Its Alteration by Organic and Inorganic Structure-Directing Agents. *Chem. Mater.* **2020**, *32*, 9277−9298.
(37) Di Iorio, J. R.; Bates, S. A.; Verma, A. A.; Delgass, W. N.; Ribeiro, F. H.; Miller, J. T.; Gounder, R. The Dynamic Nature of Brønsted Acid Sites in Cu−Zeolites During NOx Selective Catalytic Reduction: Quantification by Gas-Phase Ammonia Titration. *Top. Catal.* **2015**, *58*, 424−434.
(38) Vernuccio, S.; Bickel, E. E.; Gounder, R.; Broadbelt, L. J. Microkinetic Model of Propylene Oligomerization on Brønsted Acidic Zeolites at Low Conversion. *ACS Catal.* **2019**, *9*, 8996−9008.
(39) Costa, C.; Lopes, J. M.; Lemos, F.; Ramôa Ribeiro, F. Activity−Acidity Relationship in Zeolite Y: Part 1. Transformation of Light Olefins. *J. Mol. Catal. A Chem.* **1999**, *144*, 207−220.
(40) Wulfers, M. J.; Lobo, R. F. Assessment of Mass Transfer Limitations in Oligomerization of Butene at High Pressure on H-Beta. *Appl. Catal., A* **2015**, *505*, 394−401.
(41) Weisz, P. B.; Prater, C. D.Interpretation of Measurements in Experimental Catalysis. In *Advances in Catalysis*, Frankenburg, W. G.; Komarewsky, V. I.; Rideal, E. K., Eds.; Academic Press, 1954; Vol. *6*, pp 143−196.
(42) Krishna, R.; van Baten, J. M. Diffusion of Hydrocarbon Mixtures in MFI Zeolite: Influence of Intersection Blocking. *Chem. Eng. J.* **2008**, *140*, 614−620.
(43) Li, Y.; Zhang, C.; Li, C.; Liu, Z.; Ge, W. Simulation of the Effect of Coke Deposition on the Diffusion of Methane in Zeolite ZSM-5. *Chem. Eng. J.* **2017**, *320*, 458−467.
(44) Karge, H. G.; Nießen, W.; Bludau, H. In-Situ FTIR Measurements of Diffusion in Coking Zeolite Catalysts. *Appl. Catal., A* **1996**, *146*, 339−349.
(45) Han, J.; Liu, Z.; Li, H.; Zhong, J.; Zhang, W.; Huang, J.; Zheng, A.; Wei, Y.; Liu, Z. Simultaneous Evaluation of Reaction and Diffusion over Molecular Sieves for Shape-Selective Catalysis. *ACS Catal.* **2020**, *10*, 8727−8735.
(46) Díaz, M.; Epelde, E.; Valecillos, J.; Izaddoust, S.; Aguayo, A. T.; Bilbao, J. Coke Deactivation and Regeneration of HZSM-5 Zeolite Catalysts in the Oligomerization of 1-Butene. *Appl. Catal., B* **2021**, *291*, No. 120076.
(47) Dimon, B.; Cartraud, P.; Magnoux, P.; Guisnet, M. Coking, Aging and Regeneration of Zeolites: XIV. Kinetic Study of the Formation of Coke from Propene over USHY and H-ZSM-5. *Appl. Catal., A* **1993**, *101*, 351−369.
(48) Quann, R. J.; Green, L. A.; Tabak, S. A.; Krambeck, F. J. Chemistry of Olefin Oligomerization over ZSM-5 Catalyst. *Ind. Eng. Chem. Res.* **1988**, *27*, 565−570.
(49) Martínez, C.; Corma, A. Inorganic Molecular Sieves: Preparation, Modification and Industrial Application in Catalytic Processes. *Coord. Chem. Rev.* **2011**, *255*, 1558−1580.
(50) Garwood, W. E.Conversion of C2-C10 to Higher Olefins over Synthetic Zeolite ZSM-5. In *Intrazeolite Chemistry*, Stucky, G. D.; Dwyer, F. G., Eds.; American Chemical Society: Washington, D.C., 1983; Vol. *218*, pp 383−396.
(51) Lavrenov, A. V.; Karpova, T. R.; Buluchevskii, E. A.; Bogdanets, E. N. Heterogeneous Oligomerization of Light Alkenes: 80 Years in Oil Refining. *Catal. Ind.* **2016**, *8*, 316−327.
(52) Wang, C.; Li, B.; Wang, Y.; Xie, Z. Insight into the Topology Effect on the Diffusion of Ethene and Propene in Zeolites: A Molecular Dynamics Simulation Study. *J. Energy Chem.* **2013**, *22*, 914−918.
(53) Bhore, N. A.; Klein, M. T.; Bischoff, K. B. The Delplot Technique: A New Method for Reaction Pathway Analysis. *Ind. Eng. Chem. Res.* **1990**, *29*, 313−316.

https://doi.org/10.1021/jacsau.2c00462
JACS Au 2022, 2, 2585−2595